https://doi.org/10.5194/amt-2020-279
Preprint. Discussion started: 14 August 2020

Atmospheric Measurement Techniques Discussions

High precision laser spectrometer for multiple greenhouse gas analysis in 1 mL air from ice core samples

Bernhard Bereiter[1,3], Béla Tuzson[1], Philipp Scheidegger[1,2], André Kupferschmid[2], Herbert Looser[1], Lars Mächler[3], Daniel Baggenstos[3], Jochen Schmitt[3], Hubertus Fischer[3], and Lukas Emmenegger[1]

[1]Laboratory for Air Pollution / Environmental Technology, Empa - Swiss Federal Laboratory for Materials Science and Technology, 8600 Dübendorf, Switzerland
[2]Transport at Nanoscale Interfaces, Empa - Swiss Federal Laboratory for Materials Science and Technology, 8600 Dübendorf, Switzerland
[3]Climate and Environmental Physics and Oeschger Center for Climate Research, University of Bern, 3012 Bern, Switzerland

Correspondence: Béla Tuzson (bela.tuzson@empa.ch)

Abstract. The record of past global background atmospheric greenhouse gas composition is crucial for our understanding of global climate change. The "Beyond EPICA Oldest Ice Core" project is currently pushing the frontier of this knowledge forward by the retrieval of an ice core reaching back to 1.5 million years ago. The oldest section of this core will have been strongly thinned by glacier flow with about $15\,\mathrm{kyr}$ being trapped in as little as $1\,\mathrm{m}$ thickness of ice. This reduces the available sample volume to only a few mL of air for the targeted century-scale resolution of greenhouse gas records. Under these conditions, the required accuracy for multiple greenhouse gases cannot be achieved with currently available analytical methods.

Here, we present a new approach to unlocking such challenging atmospheric archives with a high-precision mid-IR dual-laser direct absorption spectrometer. The instrument is designed to simultaneously measure CH_4, N_2O, CO_2 concentrations as well as $\delta^{13}C(CO_2)$ using discrete samples of only $1\,\mathrm{mL}$ STP, and it achieves a precision of $1.6\,\mathrm{ppb}$, $1.0\,\mathrm{ppb}$, $0.03\,\mathrm{ppm}$ and $0.04\,‰$, respectively. Repeated measurement cycles of air samples demonstrate an excellent accuracy level, and high reproducibility of the spectroscopic and the gas handling system. In addition, this non-invasive method allows reuse of the precious gas samples for further analysis, which opens new opportunities in ice core science.

1 Introduction

Precise monitoring of the current anthropogenic rise of the greenhouse gas concentrations of CO_2, CH_4 and N_2O is essential for the implementation of the Kyoto (UNFCCC, 1998) and Paris (UNFCCC, 2015) agreements, with their goal to substantially mitigate greenhouse gas emissions and limit global anthropogenic warming to well below $2\,^{\circ}\mathrm{C}$ relative to the pre-industrial era. Several monitoring networks have been established comprising both ground- and satellite-based instrumentation for accurate greenhouse gas measurements with high temporal and spatial resolution. For ground-based monitoring, where essentially unlimited sample volumes are available, continuous infrared spectroscopic analysis gained increasing importance, as it allows for high time resolution with a minimum of sample preparation and multiple greenhouse gases in a single instrument (e.g.

https://doi.org/10.5194/amt-2020-279
Preprint. Discussion started: 14 August 2020

Atmospheric Measurement Techniques Discussions

McManus et al., 2010; Hammer et al., 2013; Hundt et al., 2018). In recent years, these techniques have been further developed, also enabling isotopic measurements of CO_2, CH_4 and N_2O (e.g. Tuzson et al., 2011; Prokhorov et al., 2019; Eyer et al.; Ibraim et al., 2017).

While today's changes are precisely monitored with constantly improving global measurement networks and provide strong constraints on anthropogenic and natural emissions, such direct atmospheric observations only began in the late 1950s (Graven et al., 2013). However, for validating climate models that predict Earth's future climate, data, such as temperature and greenhouse gas concentrations, from a larger time span, i.e. over many centuries to millennia, are needed. Moreover, processes controlling the natural range and variability of greenhouse gases can only be fully identified when the greenhouse gas record is extended over the full range of climate variations, representative of long-term orbital up to weathering time scales. An extension of the observation record, spanning the last $800\,\mathrm{kyr}$, has become possible using polar ice cores, from which small samples of past atmospheric air can be extracted. Thus, a reconstruction of the CO_2, CH_4 and N_2O records over the entire anthropogenic era (Rubino et al., 2013; MacFarling Meure et al., 2006) and further back in time over past glacial-interglacial cycles covering up to the last $800\,\mathrm{kyr}$ was realized (Loulergue et al., 2008; Schilt, 2013; Bereiter et al., 2015). Apart from greenhouse gas concentrations, the precise quantification of their isotopic composition using mass spectrometric (MS) or coupled gas chromatography - mass spectrometric (GC-MS) analyses of ice core samples has become possible in recent years (Schmitt et al., 2012; Schilt et al., 2014; Bock et al., 2017; Bauska et al., 2018).

In 2019, the European "Beyond EPICA Oldest Ice Core" project was started by partners from ten European nations with the goal to retrieve a continuous Antarctic ice core going back over the last $1.5\,\mathrm{Myr}$ (Fischer et al., 2013). For the first time, this ice core will allow to reconstruct the atmospheric changes that occurred over the so-called Mid Pleistocene Transition, when the cyclicity of glacial/interglacial cycles changed from 40 to about $100\,\mathrm{kyr}$, and the amplitude of continental glaciation during ice ages substantially increased. Due to glacier flow, the ice at the bottom of the ice sheet experienced extreme thinning, i.e. about $15\,\mathrm{kyr}$ of climate history are compressed into only $1\,\mathrm{m}$ thickness of ice core (Bereiter et al., 2014; Fischer et al., 2013) thus implying a limited availability of sample for greenhouse gas and other analyses. Accordingly, these extraordinary glaciological conditions require novel analytical approaches to maximize temporal resolution of the records, while minimizing sample consumption and, at the same time, making no compromises on precision and repeatability of the gas analyses. Thus, the various greenhouse gas analyses, previously done on several pieces of ice, have to be combined and the sensitivity of the analytical methods improved, and whenever possible reuse of the gas after the analysis for other analytical purposes should be pursued.

These goals motivated the development of a multi-species laser spectrometer using state-of-the-art mid-IR quantum cascade laser (QCL) technology. This new spectrometer is accompanied by the development of a near-IR laser sublimation system to quantitatively and continuously extract the air enclosed in ice cores in 1–$2\,\mathrm{cm}$ resolution. The sublimation technique and its performance will be described in a separate paper, while here we concentrate on the description and performance of the laser spectrometer.

In the following, we present the technical details of the developed instrument including the optical design, the custom-made absorption cell and electronics, the instrument periphery as well as the custom-made standard gases needed for the calibration.

https://doi.org/10.5194/amt-2020-279
Preprint. Discussion started: 14 August 2020


Atmospheric Measurement Techniques Discussions

Finally, a detailed characterization and calibration for 1 ml STP air samples is given, demonstrating the excellent analytical capabilities of the spectrometer, and including the first steps towards a calibration scheme that can handle the variable sample volumes and pressures that are expected from ice core samples.

2 Methods

Discrete measurements of greenhouse gas concentrations in ice cores often rely on GC techniques, while isotope ratio analyses are performed by mass spectrometry. However, these methods involve tedious and time-consuming separation of individual gas species from the air matrix. As an alternative approach, the application of a mid-IR tunable diode laser spectrometer for discrete CO_2 analyses on ice cores had already been pioneered at the University of Bern already in the 1970s (Lehmann et al., 1977; Neftel et al., 1982). This technique avoids the separation of CO_2 from the gas matrix and enables high precision concentration measurements on very small ($<10\,g$ of ice) samples equivalent to $<1\,mL$ STP. It has been used for decades in numerous studies on CO_2 concentrations in ice cores (Bereiter et al., 2015, and references therein), and has been further developed towards other- and multi-species analytics (Güllük et al., 1997). Recently, cavity-enhanced near-IR laser spectroscopy was applied for continuous online measurements of CH_4 in ice cores (Chappellaz et al., 2013; Rhodes et al., 2015). However, as these analyses involve a gas separation step from a continuous water stream, solubility effects require external calibration of such melt water based online measurements.

In the atmospheric sciences, laser spectroscopy is a well-established analytical method for high-precision trace gas concentration and isotope ratio measurements. However, the stringent requirements related to ice core analysis still remain highly challenging. In the present study, our aim was to establish an analytical tool, which enables the joint quantification of CO_2, CH_4 and N_2O concentrations as well as the stable carbon isotopic composition of CO_2 on one ice core-derived air sample of only 1–2 mL STP without separation of these gases from the air matrix. The required precision targets for high-quality ice core analyses were defined as $0.1\,ppm$, $2\,ppb$, $2\,ppb$ and $0.04\,‰$ for CO_2, CH_4, N_2O, and $\delta^{13}C(CO_2)$, respectively, in order to allow for authoritative interpretation of the observed glacial/interglacial changes in the biogeochemical cycles of these three greenhouse gases. Moreover, the option of cryogenically recollecting the air sample after the laser spectroscopic analysis was also foreseen.

The targeted multi-species capabilities of our instrument is achieved by using a dual-laser concept (see e.g. McManus et al., 2011, 2015), where two distributed feedback quantum cascade lasers (DFB-QCLs) with distinct frequencies are combined and coupled into a multipass absorption cell (MPC). The lasers were selected to fulfill fundamental line selection criteria (see e.g. Tuzson et al., 2008) that consider spectral interference issues, limitations in laser tuning capabilities ($<4\,cm^{-1}$), and achievable signal-to-noise ratio (SNR) under the targeted sample conditions. Furthermore, the selection considers the fact that CH_4 and N_2O share a region of relatively strong absorption lines around $7.7\,\mu m$, which gives access to both species within the spectral coverage of one DFB-QCL. For CO_2 (including the two most abundant isotopologues), we use the region around $4.3\,\mu m$, with a special focus on absorption lines that have comparable intensities. In this spectral region, there are mainly two options for CO_2 that fulfill all the above criteria: The lines proposed by Tuzson et al. (2008) around $2310\,cm^{-1}$ and the ones around

https://doi.org/10.5194/amt-2020-279
Preprint. Discussion started: 14 August 2020

Atmospheric Measurement Techniques Discussions

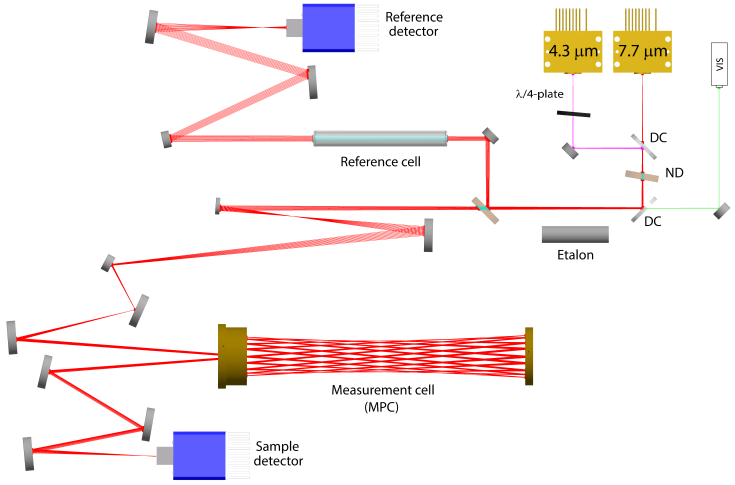

Figure 1. Optical layout of the dual-QCL system showing all relevant optical elements (where DC refers to dichroic mirror, ND to neutral density filter) and the optical path (colored lines) of the laser beams as simulated by FRED ray-tracing software (Photon Engineering).

$2302\,\mathrm{cm}^{-1}$ that we use in this work. The latter were chosen because of their higher line intensity which helps reaching the required SNR despite the small sample size.

2.1 Optical design of QCLAS

The concept and the final layout of our optical setup is shown in Fig. 1. During the development, first a 3D CAD model coupled to ray-tracing simulations was used that allowed easy testing of different design options and optimizing beam propagation within the available space. Key factors were the beam-shaping and efficient coupling of both laser beams into the same measurement cell, which is a custom-made astigmatic Herriott multipass cell (see Sect. 2.1.1) developed at Empa. Although the QCLs (Alpes Lasers, Switzerland) were packaged in a high-heat-load (HHL) housing with embedded thermoelectric cooler (TEC) and collimating lens, the output beam size and profile was not sufficiently well known. Therefore, the beam properties of each QCL were characterized in depth using a mid-IR beam profiler (WinCamD-IR-BB, DataRay, USA). The empirical values were then used to define the light sources in the ray-tracing software (FRED, Photon Engineering, USA). This allowed a more realistic beam propagation along the optical path and, thus, led to better estimates for the steering and shaping elements, which best fulfill the entrance conditions of the MPC (see e.g. McManus, 2007).

In a first section, a beam of three lasers is generated by using a custom-made dichroic mirror (LohnStar Optics, USA) to efficiently combine the two mid-IR beams first, followed by a second dichroic mirror (Quantum Design, Switzerland) to couple in a red trace laser, which is used for alignment purposes only. After the beam combination, the beam is split into two paths: a ‘sample’ path that goes through the MPC, and a ‘reference’ path, which is directed through a reference cell filled with a predefined gas mixture. The splitting ratio is such that the extra losses due to the multiple reflections within the MPC are

https://doi.org/10.5194/amt-2020-279
Preprint. Discussion started: 14 August 2020

Atmospheric Measurement Techniques Discussions

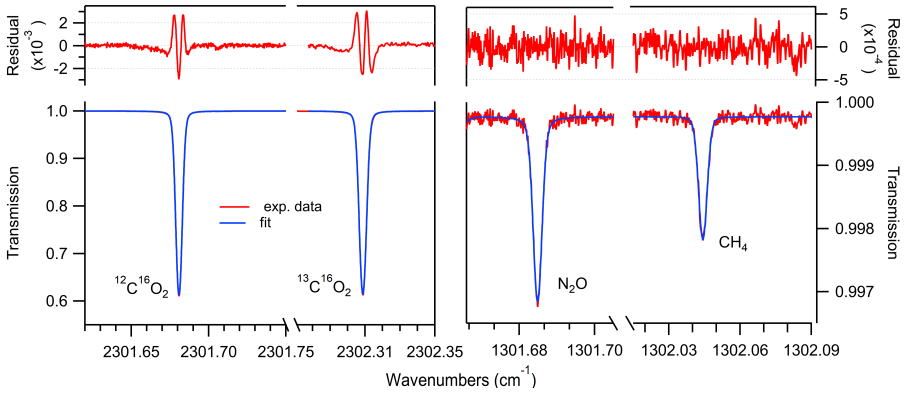

Figure 2. Example of measured transmission spectra (red), Voigt-profile fit (blue) and residual (top) for the scanned ranges at 4.3 µm (left) and 7.7 µm (right) for a gas at 5 mbar with concentrations representative of ice core samples, i.e. using standard gas #6 (see Table 1).

compensated for, and both the sample and reference detectors (Vigo Systems, Poland) receive approximately the same optical power. The optical elements downstream of the beam splitting are for beam shaping and steering. The reference cell is mounted on a remotely controllable flip-mount, and it is taken out of the beam once per measurement cycle to obtain the laser emission profile used as signal background.

Investigations of the beam properties regarding intensity and frequency stability revealed an increased sensitivity of the QCLs to optical feedback when they are driven with currents near their lasing threshold. This was more pronounced for the 4.3 µm QCL and led to marked instabilities of the emission frequency (jitter). Therefore, the QCLs are driven at high current, and a quarter wave plate is placed in the front of the 4.3 µm QCL to further reduce optical feedback. High-current operation of QCLs implies increased optical output power, which is usually beneficial in terms of SNR in the mid-IR. However, in our case the QCLs provide so much optical power (>50 mW) that (i) the linear range of the detector is exceeded, and (ii) the absorption process in the low-pressure sample gases becomes saturated. To avoid these effects, a neutral density filter (ND = 1.0) is placed between the two dichroic mirros (see also Sect. 3.3).

To decouple the optical setup from external temperature changes, the optical breadboard is water-cooled and maintained at $20 \pm 0.005\,^{\circ}\mathrm{C}$. Furthermore, the whole setup is enclosed in a sealed and thermally insulated case (Fibox, Switzerland), which is purged with CO_2-free air (resulting in a stable background of about 15 ppm CO_2) to minimize light absorption outside the sample and reference cells. These factors are significantly contributing in maintaining the long-term stability of the spectrometer.

2.1.1 Custom-made absorption gas cell

The absorption cell is a key component of any absorption laser spectrometer. It not only defines the supported optical path length (OPL), but also the volume in which the light can interact with the molecules of the sample gas. As the SNR scales with the increase of OPL, extended paths are usually achieved by using beam folding concepts, such as multipass cells (MPCs).

https://doi.org/10.5194/amt-2020-279
Preprint. Discussion started: 14 August 2020


Atmospheric Measurement Techniques Discussions

Beam folding, however, is also an important source of optical noise in the system and needs careful consideration. In our application, the precision targets of about $2\,\mathrm{ppb}$ for CH_4 and N_2O at ambient concentration and low pressure ($<10\,\mathrm{mbar}$) can be achieved with an estimated minimal optical path length of around $30\,\mathrm{m}$. These criteria are largely fulfilled by a commercially available solution (AMAC-36, Aerodyne Research, USA), which is currently the state-of-the-art MPC for high-precision trace gas measurements (McManus et al., 2010) and our first choice for the prototype instrument. However, the very limited sample volume and the aim of cryogenic re-collection of the sample after measurement create additional demands on the cell: i) it must be leak-tight on high-vacuum standards, ii) the cell inner surface must be highly inert, and iii) the cell should have a minimum dead volume. Since the AMAC-36 is primarily aimed at atmospheric monitoring applications using flow-through mode, the above aspects relevant for our purpose are not fully met. This became evident when using the AMAC-36 in static mode where we observed a continuous decrease of $0.2\,\mathrm{ppm\,min^{-1}}$ in the CO_2 concentration. Furthermore, despite the leak-tightness of the MPC, the evacuation of the cell took significantly longer compared to a simple high-vacuum-proofed volume of similar size. Hence, we concluded that these characteristics were caused by adsorption processes on the cell inner surfaces and by internally closed volumes acting as "gas buffers". The efforts of trying to fix these issues by coating the surfaces and modifying the constructional design appeared to be significant and, therefore, we decided to develop a new cell while considering all the relevant requirements mentioned above in its design.

The basic design difference of our cell with respect to the AMAC-36 is the cell-body milled from solid stainless steel, which allows to shape the cell inner surface as a cuboid that matches the envelope of the optical pattern of the laser beam between the two astigmatic mirrors. This design approach leads to a $30\,\%$ reduction of the inner volume (to $166 \pm 5\,\mathrm{cm^3}$) compared to the classical cylindrical design and thus increases the pressure of the air sample, which is crucial to reach the targeted precision. A further significant benefit of the single-piece cell body is the possibility to manufacture most of the mechanics, required for mirror mounting and aligning, out of the same piece. This allows minimizing manufacturing tolerances and reducing the degrees of freedom for mirror mounting to axial shift and rotation of only the back mirror. Furthermore, this concept simplifies the inner mechanics and helps in minimizing the dead volume.

The calculation of the geometry of the astigmatic mirror pair is based on the paraxial matrix approach (McManus et al., 1995; McManus, 2007). In general, for a given mirror geometry, there is a large number of possible reflection patterns supported for varying mirror distances and tilt angles. For the search of suitable mirror geometries, we set the following boundary conditions: i) a low volume for the targeted $30\,\mathrm{m}$ OPL, and ii) a reflection pattern that generates a minimum of optical fringes, or fringes with frequencies that substantially differ from the absorption line widths (about $100\,\mathrm{MHz}$). The first condition is well accomplished by a base length of $20\,\mathrm{cm}$ and mirror diameters of $4\,\mathrm{cm}$, i.e. for parameters very similar to the design of the commercial AMAC-36. For the second aspect, we first generated a pattern map with all possible combinations of mirror curvatures and tilt angle, and then calculated for individual patterns the spatial separation of each reflection spot with respect to its neighbors and searched for candidates with a high separation level. The expected interference frequencies were derived based on the optical path difference of the neighboring spots. In consideration of all these aspects, we selected the pattern shown in Fig. 3, which is characterized by 162 reflections. The mirrors were manufactured by diamond turning and post polishing a NiP coated aluminum substrate (LT Ultra-Precision Technology, Germany). Finally, a broadband high-reflectivity

https://doi.org/10.5194/amt-2020-279
Preprint. Discussion started: 14 August 2020

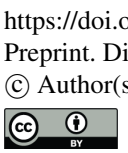

Atmospheric Measurement Techniques Discussions

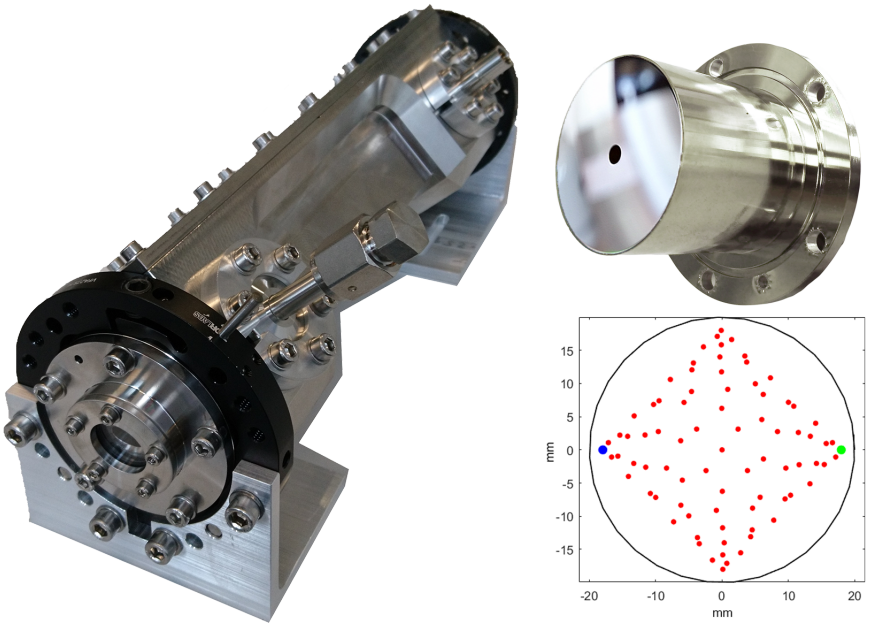

Figure 3. The low-volume and high-vacuum-sealed optical MPC developed and manufactured for the spectrometer. Left: Photograph of the cell with its entry window and the gas inlet in the foreground. Right-top: Photograph of the astigmatic mirror with the entry-hole in the center. The mirror body design allows for a direct and leak-tight attachment to the cell thereby minimizing the dead volume. Right-bottom: Reflection pattern (red dots) on the two mirrors as used in the current configuration. The blue and green dots represent the first and last reflection, respectively.

coating (Pleiger Laseroptik, Germany) was applied to achieve $99.0\,\%$ reflectivity for both selected IR-spectral ranges and $98.0\,\%$ for the visible range. The exact optical path length ($34.134 \pm 0.003\,\mathrm{m}$) was measured by coupling in a commercial laser distance meter (Disto D510, Leica Geosystems, Switzerland). The high-vacuum-proofed construction assures very low leak-rates ($<1 \times 10^{-7}\,\mathrm{mbar\,L\,s^{-1}}$) and fast pump down times (from $5\,\mathrm{mbar}$ to $0.01\,\mathrm{mbar}$ in $90\,\mathrm{s}$). This is a prerequisite for fast change-over between sample and standard which contributes to a high accuracy in applications with small, discrete samples (see Sect. 3).

2.2 Hardware design and data processing

Our laser driving and data processing electronics approach are described in detail elsewhere (Liu et al., 2018; Tuzson et al., 2020) and only a brief summary is given here. The two QCLs are driven in intermittent continuous wave (ICW) mode with time-division multiplexed timing (Fischer et al., 2014). Applying the current pulses, the laser emission frequency is rapidly tuned, allowing for complete spectral scans within $75\,\mu\mathrm{s}$. The tuning-rate is transformed into a linearized frequency scale by using the transmission spectrum of a solid Germanium etalon, which is mounted on a custom-made flip-mount. Repeated measurements

https://doi.org/10.5194/amt-2020-279
Preprint. Discussion started: 14 August 2020


Atmospheric Measurement Techniques Discussions

indicate that the QCL tuning characteristics are highly stable over time and new characterizations are only needed after major interventions into the system.

Hardware control and data acquisition electronics deployed here are similar to those of Liu et al. (2018). The main difference is that we use a more powerful programmable board (Alpha250, Koheron, France), built around a field-programmable gate array (FPGA, Zynq 7020, Xilinx), which features faster sampling rate ($250\,\mathrm{MSs}^{-1}$) and a higher bandwidth ($100\,\mathrm{MHz}$) analog front-end with dual-channel 14-bit ADCs and 16-bit DACs. This upgrade was necessary because of the required higher spectral resolution (narrow line widths due to low-pressure samples) and the dual-path configuration resulting in two simultaneous inputs to the ADC (see Fig. 4). The FPGA firmware (VHDL-Code) and the Linux service routines (C-Code) were custom developed. The FPGA contains a state-machine that is clocked eight times slower than the sample clock, which makes routing less critical, i.e. larger data path delays are tolerated. For higher flexibility in data acquisition, several user-defined time-windows within a spectral scan are supported. The summation of consecutive spectra is implemented with digital signal processors (DSP) and dual port block random access memory (BRAM). The spectra are then transferred from the programming logic via direct memory access (DMA) into the DDR-RAM of the processing unit. These data can either be sent to an external computer via a TCP/IP-interface or stored on a flash memory for post-processing.

For the spectral analysis, we used the averaged data of 5000 spectra corresponding to $1\,\mathrm{Hz}$ time resolution. In total, five acquisition windows were defined over the two laser pulses. One data acquisition window is used to record the detector signal while the lasers are not turned on yet. This signal is used to normalize the follow-up spectra that are collected in the other four windows within the laser scan. The concentrations of the individual species are retrieved by fitting a Voigt function to the measured spectra using the Levenberg-Marquardt least-squares algorithm. The spectral line intensity and the broadening parameters are taken from the HITRAN2016 database (Gordon et al., 2017), whereas the gas pressure and temperature are measured. The corresponding transmission spectra with the associated fitted curves using Voigt profiles are shown in Fig. 2.

2.3 Gas handling hardware

A fully automated gas handling system has been built around the spectrometer as depicted in Fig. 5. The system is equipped with two pumps (turbo-molecular pump station and diaphragm pump) used to pull reference gases from the cylinders through parts of the system at a steady flow, independently of the measurement cycle, or to evacuate the MPC and the manifold-line between individual discrete samples. A multi-port selector (6-port, Vici Valco Instruments Inc., Switzerland) with individual vents allows switching between the standard gas cylinders while maintaining an uninterrupted gas flow. After the multi-port selector, the standard gas is pulled through a flow restriction (critical orifice), where the pressure drops from about $2\,\mathrm{bar}$ absolute to the mbar-level. With this setup it is possible to operate the instrument both in flow through or in batch mode. In the latter the evacuated MPC is filled to any target pressure between 2.0 and $10.5\,\mathrm{mbar}$ with an uncertainty of $\pm 0.04\,\mathrm{mbar}$.

2.4 Custom-made standard gases

Direct absorption laser spectroscopy establishes a well-defined relation between the unknown amount fraction and the measured absorbance. This relation only contains directly measurable physical quantities (temperature, pressure, optical path length, line

https://doi.org/10.5194/amt-2020-279
Preprint. Discussion started: 14 August 2020

Atmospheric Measurement Techniques Discussions

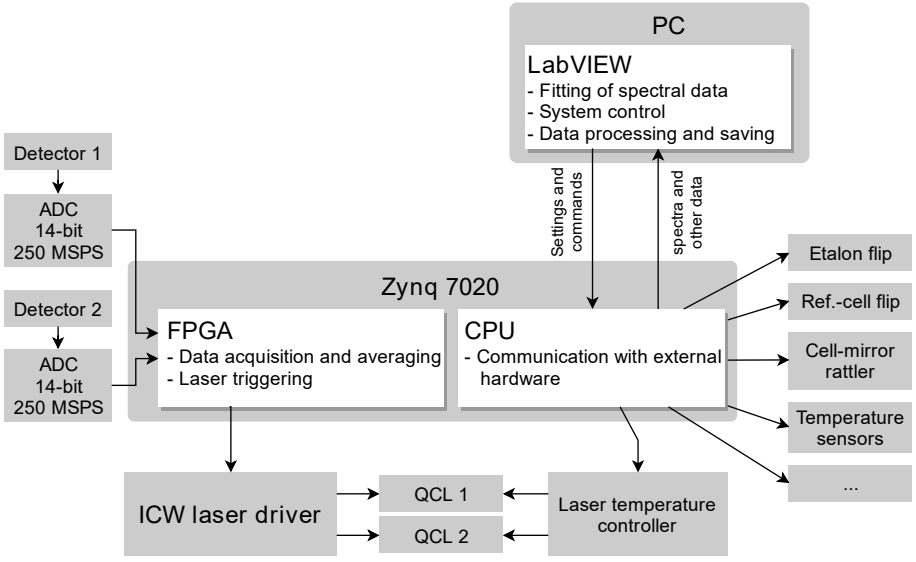

Figure 4. Schematic of the electronics setup. The core of the system is a system-on-chip (SoC) embedding a dual-core ARM processor and a FPGA, which triggers the laser driver, reads the ADCs and processes the detector signals in real-time. All processes are synchronized using the same clock generator. The hardware internal communication is based on the Inter-Integrated Circuit (I^2C) protocol. The CPU communicates with the host PC and drives other hardware, which are less critical with respect to the timing.

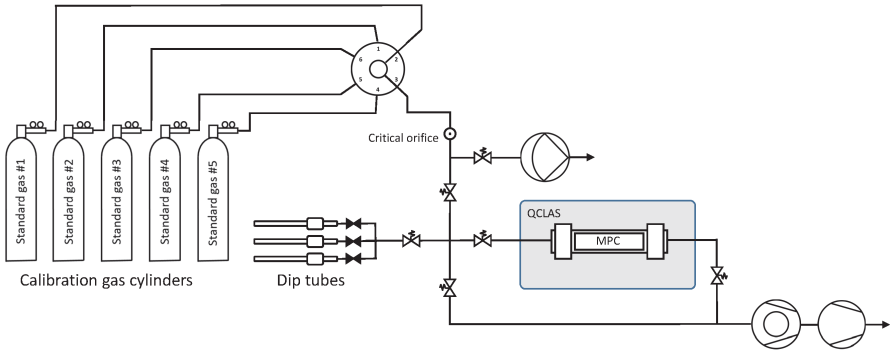

Figure 5. Gas handling system primarily used to characterize and calibrate the QCLAS instrument (schematically indicated by the gray rectangle), but also to introduce small air samples trapped in dip tubes that contain air extracted from ice core samples. The gas handling system is made out of ultra-high vacuum (UHV) stainless steel tubing and uses exclusively VCR- and KF-seals downstream of the critical orifice. The majority of the valves are pneumatically actuated valves (Fujikin Inc., Japan). For the flow-through measurements, a bypass with a metering valve (not shown) was used to reduce the flow.

amplitude) and molecular properties and thus it makes the technique – in terms of metrology – a calibration-free method
210 to determine the amount fraction of a trace gas (e.g. Buchholz et al., 2014). However, as any ”real” system, this approach

https://doi.org/10.5194/amt-2020-279
Preprint. Discussion started: 14 August 2020


Atmospheric Measurement Techniques Discussions

is also affected by, e.g. detector non-linearity, drifts, optical fringes or general instrumental response that may change over time. The relevance of these effects is gaining significance as the requirements regarding instrument performance become more stringent, which is especially pronounced for measurements of stable isotope ratios. Relatively stable and predictable instrument-related artifacts can be accounted for by a well-designed calibration scheme, which may also provide traceability to SI-units or an established calibration scale. A widely-used approach is multi-dimensional bracketing with reference gases of known isotopic composition. This targets the most critical dependencies and seeks to link the measured spectroscopic values to an international scale in a range that covers (or even goes beyond) the expected variations occurring in the samples. Relying on our previous experience in high-accuracy, traceable, long-term, and robust calibration of laser spectrometers for isotope ratio measurements (see e.g. Tuzson et al., 2011; Sturm et al., 2013), we adopted here the strategy of delta-based calibration. For this, we prepared a set of calibration gases with specific mixtures. The aim was to realize 2-dimensional bracketing for two major goals: i) reliably link the spectrally-derived isotope ratios to the internationally accepted Vienna Pee Dee Belemnite (VPDB) scale, and ii) account for the dependency of the retrieved $\delta^{13}\mathrm{C}(\mathrm{CO_2})$ values on the $\mathrm{CO_2}$ concentration (Griffith, 2018). In addition, the calibration gases were designed to also provide bracketing of the other two trace gases ($\mathrm{N_2O}$ and $\mathrm{CH_4}$). As a result, five standards were prepared, two pairs each having almost identical $\delta^{13}\mathrm{C}(\mathrm{CO_2})$ (values fixed at $-3.54\,‰$ and $-10\,‰$, respectively), but different $\mathrm{CO_2}$ concentrations covering pre-industrial/glacial-interglacial atmospheric composition ($160\,\mathrm{ppm}$ and $350\,\mathrm{ppm}$). The fifth standard gas was prepared in such a way that it falls in the middle of the corner values for both $\delta^{13}\mathrm{C}(\mathrm{CO_2})$ and $\mathrm{CO_2}$ concentration, as indicated in Fig. 6. Here, the concentrations of $\mathrm{N_2O}$ and $\mathrm{CH_4}$ (Table 1) are indicated by colors (red, green, yellow) that qualitatively reflect the respective trace-gas content (high, medium, and low).

The production of standard gases involved two main steps: (i) gravimetric production of approximate mixtures, i.e. within $10\,\%$ of the target, and (ii) subsequent quantification of these mixtures by established traceable methods. For the first step, the approximate mixtures were realized by sequentially freezing out the targeted pure greenhouse gases in cylinders, followed by dilution with greenhouse gas-free atmospheric air. The procedure in detail was: i) evacuate a $50\,\mathrm{L}$ aluminum gas cylinder, ii) place the cylinder in a liquid nitrogen bath, iii) cryogenically collect pure $\mathrm{CO_2}$ (with one or two different isotopic ratios), $\mathrm{CH_4}$ and $\mathrm{N_2O}$ from gas cylinders, iv) cryogenically collect matrix air using a modified lab-internal zero-air generator that provided (almost) greenhouse gas-free atmospheric air with unchanged $\mathrm{N_2/O_2/Ar}$ ratio. This is an important aspect to avoid any potential bias caused by uncertainties in pressure broadening effects of these species (e.g. Nara et al., 2012). One important advantage of this cryogenic trapping is that it enables the production of large volumes ($6500\,\mathrm{L}$ STP) of standard gases (see Table 1) because the gas cylinders can be filled up to their maximum filling pressure limit ($200\,\mathrm{bar}$). This permits the production of a set of cylinders with standard gases that will last for many years. In a second step, the cylinders were analyzed against NOAA/ESRL standards at the World Calibration Centre (WCC) at Empa for $\mathrm{CO_2}$, $\mathrm{CH_4}$ (CRDS, G1301, Picarro Inc., USA) and $\mathrm{N_2O}$ (QC-TILDAS, Aerodyne Research Inc., USA) concentrations several times over the following weeks to investigate potential drift effects that may appear due to the cryogenic filling. The results show that all cylinders provide stable concentrations after less than two weeks. The $\delta^{13}\mathrm{C}(\mathrm{CO_2})$ isotope ratios were analyzed at the University of Bern (Switzerland) against JRAS-06 reference gases (Wendeberg et al., 2013; Van Der Laan-Luijkx et al., 2013).

https://doi.org/10.5194/amt-2020-279
Preprint. Discussion started: 14 August 2020

Atmospheric Measurement Techniques Discussions

Table 1. List of custom-made standard gases produced for the calibration of the QCLAS. The concentrations and isotope ratio values cover the range of expected variations found in ancient air samples from ice cores. The standard #2 is only matrix air that was used to generate the various standard mixtures. The uncertainty of the values are given in parentheses.

Cylinder #	CO_2 (ppm)	CH_4 (ppb)	N_2O (ppb)	$\delta^{13}C(CO_2)$ (‰)
1.	248.8 (0.01)	528.6 (0.05)	242.0 (0.250)	-6.64 (0.037)
2.	0.2 (0.01)	0.1 (0.04)	172.7 (0.100)	n.a.
3.	157.7 (0.02)	331.2 (0.04)	189.2 (0.310)	-3.72 (0.015)
4.	167.0 (0.02)	811.0 (0.03)	340.4 (0.020)	-9.88 (0.017)
5.	345.5 (0.03)	779.8 (0.14)	325.7 (0.040)	-3.70 (0.023)
6.	239.2 (0.03)	527.2 (0.08)	236.4 (0.280)	-6.66 (0.020)
7.	341.8 (0.05)	339.2 (0.07)	167.4 (0.330)	-10.07 (0.014)

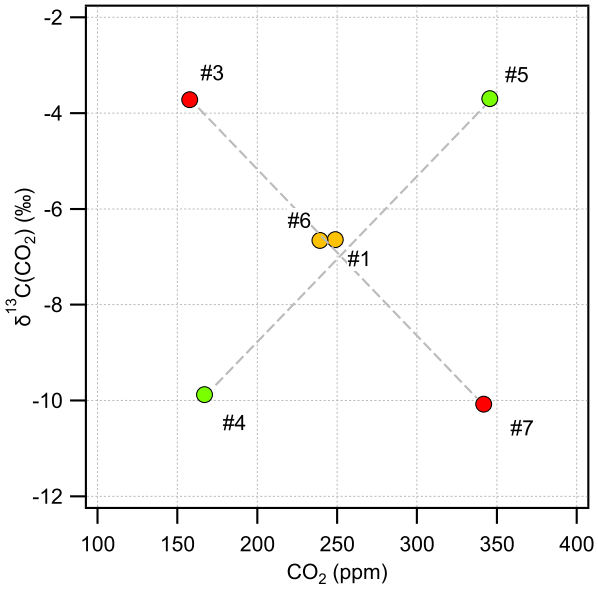

Figure 6. Range of CO_2 concentration and $\delta^{13}C(CO_2)$ isotope ratio spanned by our custom-made standard gases. The CH_4 and N_2O content is indicated by the different colors: red, green and yellow representing high-, medium-, and low-concentrations, respectively (see also Table 1).

https://doi.org/10.5194/amt-2020-279
Preprint. Discussion started: 14 August 2020


Atmospheric Measurement Techniques Discussions

3 Performance and Calibration

3.1 Precision and stability in flow-through mode

The precision and long-term stability of the system is derived with a reference gas continuously flowing through the instrument. A standard gas (#6) was continuously supplied to the MPC at a constant pressure of $5\,\mathrm{mbar}$ (corresponding to cell volume of about $1\,\mathrm{ml}$ STP) and a flow of $7\,\mathrm{mL\,min^{-1}}$ over twelve hours. In this regime, potential artefacts due to sorption effects on surfaces are mostly negligible.

Figure 7 shows the results of an Allan-Werle variance analysis (Werle, 2011) of the time-series for all four parameters. The data follow a white noise behavior for about $100\,\mathrm{s}$, except for CO_2, which flattens out already after $10\,\mathrm{s}$, and then stays at low values until at least $400\,\mathrm{s}$ before drifts begin dominating the measurements. This information is crucial for an accurate calibration because it determines the time available for the analytical cycle, i.e. the time interval within which a sample-standard measurement has to be performed. Our setup requires about $300\,\mathrm{s}$ to completely evacuate the MPC and subsequently fill it with a standard gas (see Sect. 3.2), and it is thus well matched with the above constraint. This illustrates the importance of the improved leak-tightness and minimal surface interactions of the custom-made MPC.

In parallel to the measurements in the MPC, data from the reference cell were also recorded. For CO_2, CH_4 and N_2O, only a marginal correlation between the two time-series was found. Thus, normalization with the reference cell did not improve the performance. The situation is slightly different for $\delta^{13}C(CO_2)$, where the Allan-Werle deviation minimum could be improved towards longer integration times ($>100\,\mathrm{s}$) by using the reference cell records to apply a drift correction in the form of a simple subtraction of the reference cell mean-normalized data from the MPC data. Therefore, the reference cell data can mainly be used for monitoring purposes, i.e. to efficiently flag out periods with daily variations that eventually can happen and optionally to slightly improve the precision of $\delta^{13}C(CO_2)$.

Overall, the precision targets for all the four parameters (see Sect. 2) are reached within $10\,\mathrm{s}$ integration. The instrument achieves a precision of $0.4\,\mathrm{ppb}$, $0.1\,\mathrm{ppb}$, $6\,\mathrm{ppb}$, and $0.02\,‰$ for CH_4, N_2O, CO_2, and $\delta^{13}C(CO_2)$, respectively, when integrating over 100 s.

3.2 Repeatability of discrete 1 mL STP samples

The final application of the instrument is the accurate (SI-traceable) measurement of discrete, very small air samples that need to be measured in batch mode due to their low volume. As mentioned above, the Allan-Werle deviation analysis indicates that for highest accuracy the sample-standard measurement should take place within $400\,\mathrm{s}$. The gas inlet system (see Fig. 5) was developed to allow the corresponding rapid switching between gases, while maintaining a precise pressure matching within $\pm 0.04\,\mathrm{mbar}$. For the removal of the gas from the MPC we also consider the specific ice core application, which foresees the option to cryogenically recollect the gas sample after the spectroscopic measurement in a cold finger for further MS analysis. Therefore, the sample gas is not simply flushed out of the cell with the stream of the following standard gas, but rather we evacuate the cell using the turbo-molecular pump to levels near to the detection limit of the cell pressure gauge ($10^{-3}\,\mathrm{mbar}$),

https://doi.org/10.5194/amt-2020-279
Preprint. Discussion started: 14 August 2020

Atmospheric Measurement Techniques Discussions

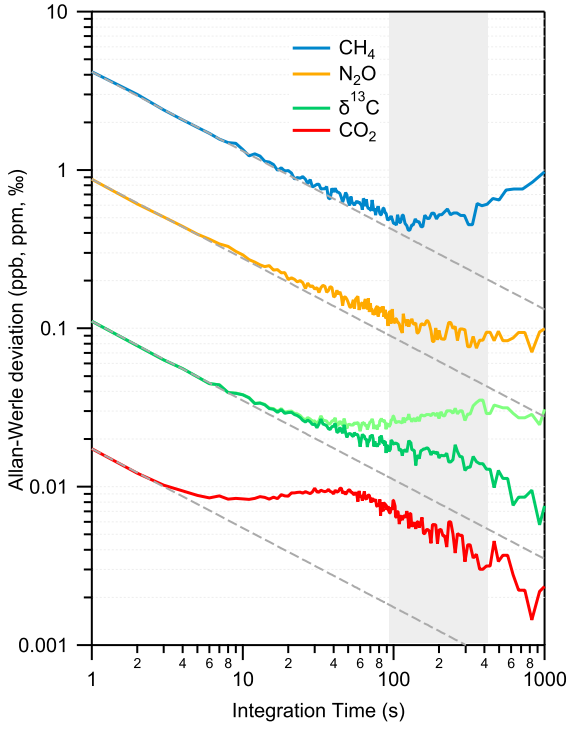

Figure 7. Allan-Werle deviation plot for all observed parameters in a flow-through experiment using the standard gas #6. For $\delta^{13}C(CO_2)$, two situations are shown: i) no drift correction (light green) and ii) applying a drift correction based on the reference cell (dark green). While in the case of isotope ratio values a slight improvement towards longer integration time can be observed, the concentrations are only marginally influenced (not shown). The optimal integration time is indicated by the gray area.

which is similar to the case of a cryogenic recollection. The total delay time between the sample and the standard is around 270 s, which is acceptable regarding the stability of the system (Fig. 7) and our precision targets (Sect. 2).

To evaluate the repeatability of discrete sample measurements of 1 ml STP volume, the following procedure is used: First, a dip tube is filled with about 1 ml STP of a standard gas, and then expanded into the evacuated MPC and treated as the 'sample' in the evaluation procedure. Second, for the 'standard' measurement, the MPC is evacuated again, and the same standard gas is introduced directly, i.e. not via dip tube, until reaching the same cell pressure. This sequence is repeated several times (50 ×) and consecutively applied for low-, mid- and high-concentration trace gas standards (see Fig. 6). To minimize potential biases originating from long-term optical drifts, we recorded spectra with evacuated cell ('zero trace') at the beginning of each sample-standard pair, which were then subtracted from consecutive spectra. This strategy efficiently removes residual structures in the spectrum that can slowly vary with time and influence the spectral fit.

The result of this experiment is summarized in Fig. 8. We found a 1 σ standard deviation of 2.2 ppb, 0.7 ppb, 0.03 ppm and 0.04 ‰ for CH_4, N_2O, CO_2 and $\delta^{13}C(CO_2)$, respectively. These values are higher by a factor 2 for $\delta^{13}C(CO_2)$, 5 for CH_4 and CO_2, and 10 for N_2O than those derived from the Allan-Werle deviation analysis of the flow-through measurements (see

https://doi.org/10.5194/amt-2020-279
Preprint. Discussion started: 14 August 2020

Atmospheric Measurement Techniques Discussions

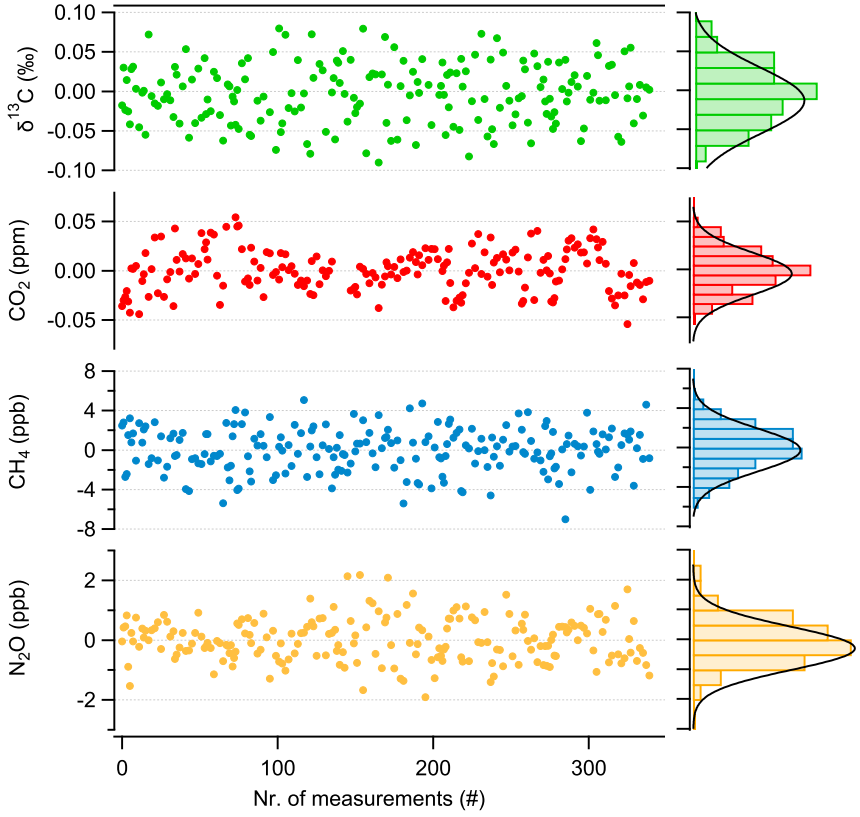

Figure 8. Repeatability of discrete sample measurements (mean value subtracted) of 1 ml STP volume with associated histograms showing the distribution of the values. These indicate normally distributed data. The bins were chosen as follows: 0.02 for $\delta^{13}C(CO_2)$, 0.01 for CO_2, 1 for CH_4, and 0.5 for N_2O.

Fig. 7). Although this trend is expected, the results indicate that significant uncertainty is introduced by the evacuation and the gas flows (e.g. temperature, mechanical stress), as well as by the gas handling process (e.g. adsorption/desorption). Overall, the accuracy is not limited by the purely spectroscopic performance, indicating that further improvements may be possible by optimizing the sample handling. Nevertheless, the targets are achieved for all compounds, even for discrete samples of only 1 ml STP volume, and this spectroscopic performance is maintained at least over 24 h of continuous operation.

3.3 Calibration characteristics of discrete 1 mL STP samples

In this section, we investigate the characteristics of the instrument response using the custom-made and externally calibrated standard gases and derive corresponding calibration functions for discrete 1 ml STP air samples. We use the same measurement procedure as described in sect. 3.2. The only difference is that the sample gas is not transferred via the dip tube but introduced directly into the MPC in the same way as the standard gas. In other words, the sample-standard pair are basically identical

https://doi.org/10.5194/amt-2020-279
Preprint. Discussion started: 14 August 2020


Atmospheric Measurement Techniques Discussions

measurements with the same gas at the same pressure ($5\,\mathrm{mbar}$). Thus, half of the data were used to monitor potential drifts in the spectrometer response, while the other half served to retrieve the target parameters. First, the values of each category ('anchor' and 'sample') are averaged for $100\,\mathrm{s}$ and then, whenever long-term drifts are larger than $3\,\sigma$ of the uncertainty of individual values, the drifts are taken into account by applying a smoothing-spline over all 'anchor' values considering their individual standard deviation as weighing factor for the spline, and setting the smoothing factor to unity (Igor Pro v8, Wavemetrics Inc., USA). After drift correction, the ten individual 'sample' values of each standard are averaged and plotted against their reference value, as shown in Fig. 9. Thereby, we found that a linear calibration function describes properly the instrument response for all three trace gas concentrations. For $\delta^{13}\mathrm{C}(\mathrm{CO_2})$, the calibration is a two-step process as its concentration dependence should also be considered (see e.g. Tuzson et al., 2008). This concentration dependence of $\delta^{13}\mathrm{C}(\mathrm{CO_2})$ is determined based on the measurements of standard gases #3 and #5 (see Table 1). As both standard gases have the same $\mathrm{CO_2}$ isotopic composition, the apparent difference observed in the spectroscopically-derived isotope ratios is assumed to be entirely due to the difference in the $\mathrm{CO_2}$ concentration. This two-point calibration, which was found to be about $0.005\,‰\,\mathrm{ppm}^{-1}$, is then applied to all the other $\delta^{13}\mathrm{C}(\mathrm{CO_2})$ values obtained for the different standard gases. Thus, the specific calibration functions of all four parameters are defined as follows:

$$[\mathrm{X}]_{cal} = a_0 + a_1 \cdot [\mathrm{X}]_{meas} \tag{1}$$

$$\delta^{13}\mathrm{C}_{cal} = d_0 + d_1 \cdot \delta^{13}\mathrm{C}_{meas} + d_2 \cdot [\mathrm{CO_2}]_{meas} \tag{2}$$

where, the subscripts '$meas$' and 'cal' denote the measured and the calibrated values, [X] stands for $\mathrm{CO_2}$, $\mathrm{CH_4}$ and $\mathrm{N_2O}$ concentrations, while a_i, and d_i represent the fit coefficients. Figure 9 shows the calibration functions and the resulting residuals for all four parameters.

Although, the spectroscopically-retrieved concentrations show a good linear correlation with the reference values, a systematic underestimation is observed, which in case of $\mathrm{CO_2}$ is $5\,\%$. This is slightly more than expected based on propagating errors in spectral (e.g. line intensity) and physical (pressure, temperature and OPL) parameters. As all species show similar characteristics, it is most likely an indication for a common underlying bias. There are mainly two effects that could contribute to such a bias: i) the Voigt profile used to fit the absorption lines tends to underestimate the effective absorption line areas especially at low pressure, and ii) the absorption lines might be slightly saturated by the incident laser optical power. Underestimation by the Voigt profile is well documented, however the literature suggests a bias between 1–2 % for our working pressure (Bui et al., 2014; Lisak et al., 2015) and thus only partly explains our observation. There is, however, strong evidence that optical saturation plays a significant role, despite the implemented intensity reduction scheme (see Sect. 2.1). This is supported by the observation that increasing cell pressure leads to an increasing slope of the calibration functions (see Fig. 10), which is in line with the expected behavior of optical saturation; higher gas pressure means higher collision rate, which causes faster relaxation of the states and ultimately reduces the number of molecules that are in the excited state. Nevertheless, the systematic error caused by this effect is included in the calibration process, because the main factors that have an impact on saturation are kept constant, e.g. temperature, pressure, laser intensity or gas matrix. To verify this assumption, we determined the instrument response to our standards in five sets of experiments, with about two-week or more time lag between each. Each set of experi-

https://doi.org/10.5194/amt-2020-279
Preprint. Discussion started: 14 August 2020

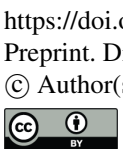

Atmospheric Measurement Techniques Discussions

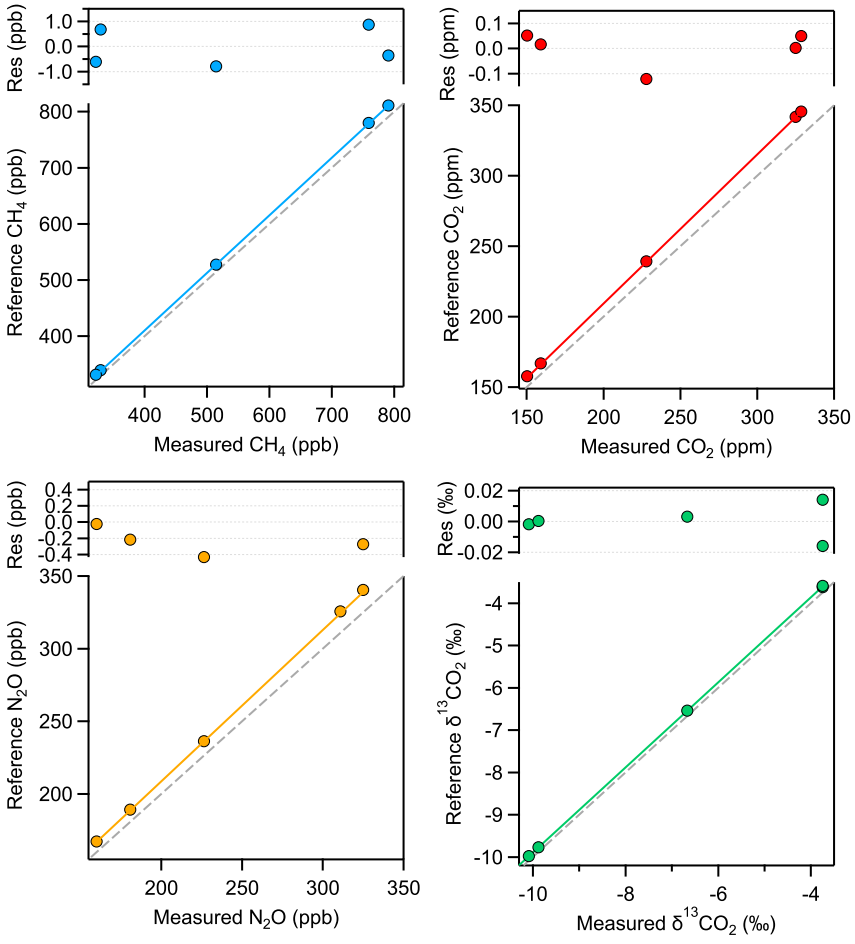

Figure 9. Calibration functions and corresponding residuals from the fit of all four analyzed parameters for a sample with 1 ml STP volume, corresponding to 5 mbar pressure in the MPC. The dashed gray lines indicate the 1:1 correlation as reference.

ments involved repeated evacuation/filling cycles of the MPC, and every standard gas was measured twenty times in a scheme as described above. We found excellent agreement across all these measurements, which demonstrates the constant analytical performance of the instrument.

It should be noted that the amount of gas resulting from ice core samples, and thus the sample pressure in the MPC, may slightly fluctuate, depending on the air content of the sublimated ice core. At the high level of required accuracy, this may be a critical parameter. Preliminary tests with the sampling and calibration procedure described here were performed to investigate the influence of gas pressure variation on the spectroscopically-retrieved values. For this, we repeated the same procedure that was used for the calibration measurements with the only difference this time being that the 'sample' measurements were done at various pressures covering the range between 2 and 10.5 mbar. Figure 10 shows the representative results for one

https://doi.org/10.5194/amt-2020-279
Preprint. Discussion started: 14 August 2020

Atmospheric Measurement Techniques Discussions

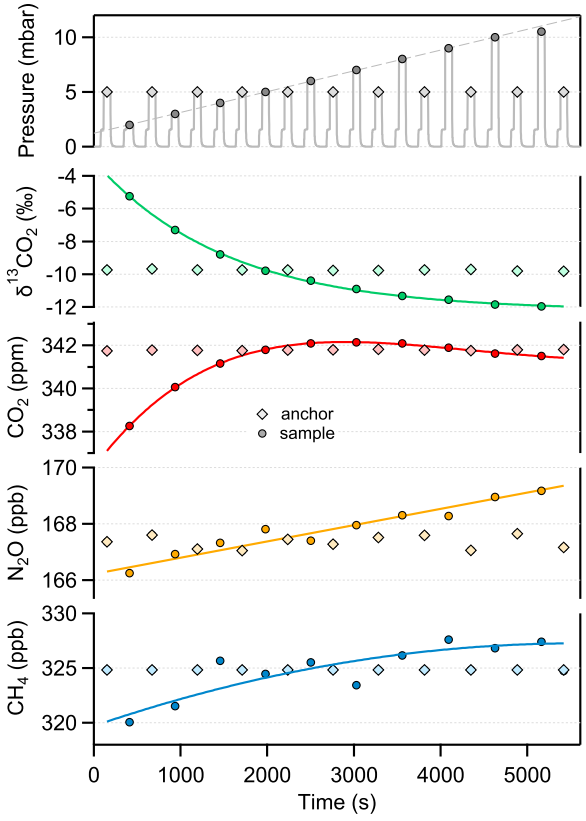

Figure 10. Pressure dependence of the target parameters. The same standard gas is used alternately as 'anchor' (diamond) and 'sample' (circle). The gas pressure for the 'anchor' is kept at 5 mbar, while the pressure of the 'sample' is gradually changed between 2 and 10 mbar (top plot). The markers represent the mean value of the measurements taken at each pressure value over 70 s. The overall sequence is repeated three times for the same standard gas and then consecutively applied to the other five standards. The instrumental response remained stable during the entire measurement time (>25 h).

standard gas. This indicates that basically every target parameter is affected by changing cell pressure. Whilst, for the CH_4 and N_2O concentration retrieval the influence of pressure is about $0.76(19)\,\mathrm{ppb\,mbar^{-1}}$ and $0.31(3)\,\mathrm{ppb\,mbar^{-1}}$, respectively, the $\delta^{13}C(CO_2)$ and the CO_2 concentration values show a strong and non-linear dependence, especially towards lower cell pressures (<5 mbar). Obviously, this effect can significantly deteriorate the spectrometer accuracy if it is not taken into account properly. Therefore, the pressure either has to be actively controlled or considered in the data retrieval. In the former case, an additional buffer volume with flexible bellows can be added to the gas-handling system to precisely adjust the cell pressure to a preset value for any ice core sample. Otherwise, the calibration functions have to be known for each pressure value. This is feasible because the pressure dependency of the target parameters have smooth characteristics and can be described by simple analytical functions (linear, polynomial or exponential). These relations hold also for the calibration function coefficients, which can then include a pressure-dependence correction term. Although, it involves a slightly higher complexity, such an

https://doi.org/10.5194/amt-2020-279
Preprint. Discussion started: 14 August 2020


Atmospheric Measurement Techniques Discussions

approach was tested successfully using interpolated calibration function coefficients for a randomly taken pressure value. Nevertheless, the final accuracy of the measurement will sensitively depend on the uncertainty from the extrapolation between the used individual calibration functions. Therefore, the best practice is still to establish an experimental solution, which maintains the cell pressure of the different samples and standard gases identical, possibly at values $\geq 5\,\mathrm{mbar}$. Furthermore, it is advisable to use standard gases that are similar to the unknown sample in both concentration and isotopic composition. Fulfilling these two conditions, the spectrometer accuracy would approach its precision level. For the ice core application, a more detailed characterization and validation of the calibration parameters in the desired pressure range is required. Here, we provided the instrument behavior over the whole possible operation range, which can build the basis for future work with this spectrometer in its final configuration including the ice core extraction system.

4 Conclusions

A dual-QCL direct absorption spectrometer has been developed for the challenging measurements of small ($1\,\mathrm{ml}$ STP) ice core samples. The stringent requirements in precision and accuracy were met by the design, development and implementation of the following key elements: i) a new low-volume multipass absorption cell was designed with a special focus on minimizing contamination effects (e.g. surface adsorption, outgassing, leak-rate), improving optical performance (low fringe level) and robustness against mechanical and thermal variations; ii) a custom-made low-noise/low-drift laser driving electronics stabilized by a thermoelectrically cooled water-loop; iii) a fast dual-channel real-time data acquisition system based on FPGA SoC; and iv) a dedicated system-tailored and automated gas handling manifold to manipulate low-volume samples.

Flow-through experiments demonstrate an analytical precision of $6\,\mathrm{ppb}$ for CO_2, $0.02\,‰$ for $\delta^{13}C(CO_2)$, $0.4\,\mathrm{ppb}$ for CH_4 and $0.1\,\mathrm{ppb}$ for N_2O obtained after an integration time of $100\,\mathrm{s}$. Sample-standard repeatabilities of discrete samples of $1\,\mathrm{ml}$ STP meet or even exceed our precision targets. Furthermore, calibration curves have been determined and verified in repeated measurements over a time span of several months and it was found that the instrument can provide calibrated values with uncertainties similar to the repeatabilities. Thus, the spectrometer is capable of simultaneously and accurately analyzing discrete air samples for their CO_2, $\delta^{13}C(CO_2)$, CH_4 and N_2O composition even at 1–2 ml STP volume as expected from future ice core samples. Being a non-invasive analytical tool, it also allows to reuse the measured sample for further analysis. Therefore, this new instrument is an ideal tool for future ice core research as targeted by the planned drilling of a $1.5\,\mathrm{Myr}$ old ice core from Antarctica.

Data availability. The data used in this manuscript are available from the corresponding author upon request.

Author contributions. B.B. designed and developed the instrument under the guidance of B.T. and with input by L.E. and H.F., while L.M., D.B., and J.S. realized the gas handling system. B.B., L.M., D.B., and J.S. performed the experiments and evaluated the data. P.S. designed

https://doi.org/10.5194/amt-2020-279
Preprint. Discussion started: 14 August 2020


Atmospheric Measurement Techniques Discussions

and developed the electronics hardware. A.K. developed and implemented FPGA and DAQ functionalities. H.L. developed the spectral analysis and hardware control software. H.F together with L.E. and B.T. designed the research, managed and supervised the project, and discussed the results. B.B. and B.T. prepared the manuscript with contributions from all authors.

Competing interests. The authors declare that they have no conflict of interest.

Acknowledgements. We acknowledge Nicolas Sobanski and Oleg Aseev for their support in designing the multipass cell mirrors. We thank Erich Heiniger from the Empa workshop for the design and construction of the MPC. Christoph Zellweger and Martin Vollmer are acknowledged for supporting and supervising the preparation of the custom-made standard gases. Markus Leuenberger and his team from University of Bern (Switzerland) is acknowledged for performing the IRMS measurements on our custom-made standards. This study is part of the ERC Advanced Grant "deepSLice" (667507) of H.F. This project has received funding from the European Research Council (ERC) under the European Union's Horizon 2020 research and innovation programme (grant agreement No [667507]).

https://doi.org/10.5194/amt-2020-279
Preprint. Discussion started: 14 August 2020

Atmospheric Measurement Techniques Discussions

References

Bauska, T. K., Brook, E. J., Marcott, S. A., Baggenstos, D., Shackleton, S., Severinghaus, J. P., and Petrenko, V. V.: Controls on Millennial-Scale Atmospheric CO_2 Variability During the Last Glacial Period, Geophysical Research Letters, 45, 7731–7740, https://doi.org/10.1029/2018GL077881, 2018.

Bereiter, B., Fischer, H., Schwander, J., and Stocker, T. F.: Diffusive equilibration of N_2, O_2 and CO_2 mixing ratios in a 1.5-million-years-old ice core, The Cryosphere, 8, 245–256, https://doi.org/10.5194/tc-8-245-2014, 2014.

Bereiter, B., Eggleston, S., Schmitt, J., Nehrbass-Ahles, C., Stocker, T., Fischer, H., Kipfstuhl, S., and Chappellaz, J.: Revision of the EPICA Dome C CO_2 record from 800 to 600-kyr before present, Geophysical Research Letters, 42, 542–549, https://doi.org/10.1002/2014GL061957, 2015.

Bock, M., Schmitt, J., Beck, J., Seth, B., Chappellaz, J., and Fischer, H.: Glacial/interglacial wetland, biomass burning, and geologic methane emissions constrained by dual stable isotopic CH_4 ice core records, Proceedings of the National Academy of Sciences, 114, E5778–E5786, https://doi.org/10.1073/pnas.1613883114, 2017.

Buchholz, B., Böse, N., and Ebert, V.: Absolute validation of a diode laser hygrometer via intercomparison with the German national primary water vapor standard, Applied Physics B: Lasers and Optics, 116, 883–899, https://doi.org/10.1007/s00340-014-5775-4, 2014.

Bui, T. Q., Long, D. A., Cygan, A., Sironneau, V. T., Hogan, D. W., Rupasinghe, P. M., Ciuryło, R., Lisak, D., and Okumura, M.: Observations of Dicke narrowing and speed dependence in air-broadened CO_2 lineshapes near 2.06 μm, Journal of Chemical Physics, 141, https://doi.org/10.1063/1.4900502, http://dx.doi.org/10.1063/1.4900502, 2014.

Chappellaz, J., Stowasser, C., Blunier, T., Baslev-Clausen, D., Brook, E. J., Dallmayr, R., Fain, X., Lee, J. E., Mitchell, L. E., Pascual, O., Romanini, D., Rosen, J., and Schüpbach, S.: High-resolution glacial and deglacial record of atmospheric methane by continuous-flow and laser spectrometer analysis along the NEEM ice core, Climate of the Past, 9, 2579–2593, https://doi.org/10.5194/cp-9-2579-2013, 2013.

Eyer, S., Tuzson, B., Popa, M. E., Van Der Veen, C., Röckmann, T., Rothe, M., Brand, W. A., Fisher, R., Lowry, D., Nisbet, E. G., Brennwald, M. S., Harris, E., Zellweger, C., Emmenegger, L., Fischer, H., and Mohn, J.: Real-time analysis of δ^{13}C- and D-CH_4 in ambient air with laser spectroscopy: Method development and first intercomparison results, Atmospheric Measurement Techniques, pp. 263–280, https://doi.org/10.5194/amt-9-263-2016.

Fischer, H., Severinghaus, J., Brook, E., Wolff, E., Albert, M., Alemany, O., Arthern, R., Bentley, C., Blankenship, D., Chappellaz, J., Creyts, T., Dahl-Jensen, D., Dinn, M., Frezzotti, M., Fujita, S., Gallee, H., Hindmarsh, R., Hudspeth, D., Jugie, G., Kawamura, K., Lipenkov, V., Miller, H., Mulvaney, R., Parrenin, F., Pattyn, F., Ritz, C., Schwander, J., Steinhage, D., van Ommen, T., and Wilhelms, F.: Where to find 1.5 million yr old ice for the IPICS "Oldest-Ice" ice core, Climate of the Past, 9, 2489–2505, https://doi.org/10.5194/cp-9-2489-2013, 2013.

Fischer, M., Tuzson, B., Hugi, A., Brönnimann, R., Kunz, A., Blaser, S., Rochat, M., Landry, O., Müller, A., and Emmenegger, L.: Intermittent operation of QC-lasers for mid-IR spectroscopy with low heat dissipation: tuning characteristics and driving electronics, Optics Express, 22, 7014, https://doi.org/10.1364/oe.22.007014, 2014.

Gordon, I. E., Rothman, L. S., Hill, C., Kochanov, R. V., Tan, Y., Bernath, P. F., Birk, M., Boudon, V., Campargue, A., Chance, K. V., Drouin, B. J., Flaud, J. M., Gamache, R. R., Hodges, J. T., Jacquemart, D., Perevalov, V. I., Perrin, A., Shine, K. P., Smith, M. A., Tennyson, J., Toon, G. C., Tran, H., Tyuterev, V. G., Barbe, A., Császár, A. G., Devi, V. M., Furtenbacher, T., Harrison, J. J., Hartmann, J. M., Jolly, A., Johnson, T. J., Karman, T., Kleiner, I., Kyuberis, A. A., Loos, J., Lyulin, O. M., Massie, S. T., Mikhailenko, S. N., Moazzen-Ahmadi, N., Müller, H. S., Naumenko, O. V., Nikitin, A. V., Polyansky, O. L., Rey, M., Rotger, M., Sharpe, S. W., Sung, K., Starikova, E., Tashkun,

https://doi.org/10.5194/amt-2020-279
Preprint. Discussion started: 14 August 2020

S. A., Auwera, J. V., Wagner, G., Wilzewski, J., Wcisło, P., Yu, S., and Zak, E. J.: The HITRAN2016 molecular spectroscopic database, Journal of Quantitative Spectroscopy and Radiative Transfer, 203, 3–69, https://doi.org/10.1016/j.jqsrt.2017.06.038, 2017.

Graven, H. D., Keeling, R. F., Piper, S. C., Patra, P. K., Stephens, B. B., Wofsy, S. C., Welp, L. R., Sweeney, C., Tans, P. P., Kelley, J. J., Daube, B. C., Kort, E. A., Santoni, G. W., and Bent, J. D.: Enhanced Seasonal Exchange of CO_2 by Northern Ecosystems Since 1960, Science, 341, 1085–1089, https://doi.org/10.1126/science.1239207, http://www.sciencemag.org/cgi/doi/10.1126/science.1239207, 2013.

Griffith, D. W.: Calibration of isotopologue-specific optical trace gas analysers: A practical guide, Atmospheric Measurement Techniques, 11, 6189–6201, https://doi.org/10.5194/amt-11-6189-2018, 2018.

Güllük, T., Wagner, H. E., and Slemr, F.: A high-frequency modulated tunable diode laser absorption spectrometer for measurements of CO_2, CH_4, N_2O, and CO in air samples of a few cm^3, Review of Scientific Instruments, 68, 230–239, https://doi.org/10.1063/1.1147814, 1997.

Hammer, S., Griffith, D., Konrad, G., Vardag, S., Caldow, C., and Levin, I.: Assessment of a multi-species in situ FTIR for precise atmospheric greenhouse gas observations, Atmospheric Measurement Techniques, 6, 1153–1170, https://doi.org/10.5194/amt-6-1153-2013, 2013.

Hundt, P., Tuzson, B., Aseev, O., Liu, C., Scheidegger, P., Looser, H., Kapsalidis, F., Shahmohammadi, M., Faist, J., and Emmenegger, L.: Multi-species trace gas sensing with dual-wavelength QCLs, Applied Physics B: Lasers and Optics, 124, https://doi.org/10.1007/s00340-018-6977-y, 2018.

Ibraim, E., Harris, E., Eyer, S., Tuzson, B., Emmenegger, L., Six, J., and Mohn, J.: Development of a field-deployable method for simultaneous, real-time measurements of the four most abundant N_2O isotopocules, Isotopes in Environmental and Health Studies, 54, 1–15, https://doi.org/10.1080/10256016.2017.1345902, 2017.

Lehmann, B., Wahlen, M., Zumbrunn, R., Oeschger, H., and Schnell, W.: Isotope analysis by infrared laser absorption spectroscopy, Applied Physics, 13, 153–158, https://doi.org/10.1007/BF00882474, 1977.

Lisak, D., Cygan, A., Bermejo, D., Domenech, J. L., Hodges, J. T., and Tran, H.: Application of the Hartmann-Tran profile to analysis of H_2O spectra, Journal of Quantitative Spectroscopy and Radiative Transfer, 164, 221–230, https://doi.org/10.1016/j.jqsrt.2015.06.012, http://dx.doi.org/10.1016/j.jqsrt.2015.06.012, 2015.

Liu, C., Tuzson, B., Scheidegger, P., Looser, H., Bereiter, B., Graf, M., Hundt, M., Aseev, O., Maas, D., and Emmenegger, L.: Laser driving and data processing concept for mobile trace gas sensing: Design and implementation, Review of Scientific Instruments, 065107, https://doi.org/10.1063/1.5026546, 2018.

Loulergue, L., Schilt, A., Spahni, R., Masson-Delmotte, V., Blunier, T., Lemieux, B., Barnola, J.-M., Raynaud, D., Stocker, T. F., and Chappellaz, J.: Orbital and millennial-scale features of atmospheric CH_4 over the past 800,000 years, Nature, 453, 383–386, 2008.

MacFarling Meure, C., Etheridge, D., Trudinger, C., Steele, P., Langenfelds, R., van Ommen, T., Smith, A., and Elkins, J.: Law Dome CO_2, CH_4 and N_2O ice core records extended to 2000 years BP, Geophysical Research Letters, 33, https://doi.org/10.1029/2006GL026152, 2006.

McManus, J.: Paraxial matrix description of astigmatic and cylindrical mirror resonators with twisted axes for laser spectroscopy, Applied Optics, 46, 472–482, https://doi.org/10.1364/AO.46.000472, 2007.

McManus, J., Kebabian, P., and Zahniser, M.: Astigmatic mirror multipass absorption cells for long-path-length spectroscopy, Applied Optics, 34, 3336–3348, https://doi.org/10.1364/AO.34.003336, 1995.

McManus, J., Zahniser, M., Nelson Jr., D., Shorter, J., Herndon, S., Wood, E., and Wehr, R.: Application of quantum cascade lasers to high-precision atmospheric trace gas measurements, Optical Engineering, 49, https://doi.org/10.1117/1.3498782, 2010.

McManus, J. B., Zahniser, M. S., and Nelson, D. D.: Dual quantum cascade laser trace gas instrument with astigmatic Herriott cell at high pass number, Applied Optics, 50, A74, https://doi.org/10.1364/AO.50.000A74, 2011.

https://doi.org/10.5194/amt-2020-279
Preprint. Discussion started: 14 August 2020

Atmospheric Measurement Techniques Discussions

McManus, J. B., Nelson, D. D., and Zahniser, M. S.: Design and performance of a dual-laser instrument for multiple isotopologues of carbon dioxide and water, Optics Express, 23, 6569, https://doi.org/10.1364/oe.23.006569, 2015.

Nara, H., Tanimoto, H., Tohjima, Y., Mukai, H., Nojiri, Y., Katsumata, K., and Rella, C. W.: Effect of air composition (N_2, O_2, Ar, and H_2O) on CO_2 and CH_4 measurement by wavelength-scanned cavity ring-down spectroscopy: Calibration and measurement strategy, Atmospheric Measurement Techniques, 5, 2689–2701, https://doi.org/10.5194/amt-5-2689-2012, 2012.

Neftel, A., Oeschger, H., Schwander, J., Stauffer, B., and Zumbrunn, R.: Ice core sample measurements give atmospheric CO_2 content during the past 40,000 yr, Nature, 295, 220–223, https://doi.org/10.1038/295220a0, 1982.

Prokhorov, I., Kluge, T., and Janssen, C.: Optical clumped isotope thermometry of carbon dioxide, Scientific Reports, 9, https://doi.org/10.1038/s41598-019-40750-z, 2019.

Rhodes, R. H., Brook, E. J., Chiang, J. C. H., Blunier, T., Maselli, O. J., McConnell, J. R., Romanini, D., and Severinghaus, J. P.: Enhanced tropical methane production in response to iceberg discharge in the North Atlantic, Science, 6238, 1016–1019, 2015.

Rubino, M., Etheridge, D. M., Trudinger, C. M., Allison, C. E., Battle, M. O., Langenfelds, R. L., Steele, L. P., Curran, M., Bender, M., White, J. W. C., Jenk, T. M., Blunier, T., and Francey, R. J.: A revised 1000 year atmospheric δ^{13}C-CO_2 record from Law Dome and South Pole, Antarctica, Journal of Geophysical Research, pp. 8382–8499, 2013.

Schilt, A.: History of Nitrous Oxide from Ice Cores, Encyclopedia of Quaternary Science: Second Edition, pp. 471–476, https://doi.org/10.1016/B978-0-444-53643-3.00333-2, 2013.

Schilt, A., Brook, E. J., Bauska, T. K., Baggenstos, D., Fischer, H., Joos, F., Petrenko, V. V., Schaefer, H., Schmitt, J., Severinghaus, J. P., Spahni, R., and Stocker, T. F.: Isotopic constraints on marine and terrestrial N_2O emissions during the last deglaciation, Nature, 516, 234–237, https://doi.org/10.1038/nature13971, 2014.

Schmitt, J., Schneider, R., Elsig, J., Leuenberger, D., Lourantou, A., Chappellaz, J., Kohler, P., Joos, F., Stocker, T. F., Leuenberger, M., and Fischer, H.: Carbon Isotope Constraints on the Deglacial CO_2 Rise from Ice Cores, Science, 336, 711–714, https://doi.org/10.1126/science.1217161, 2012.

Sturm, P., Tuzson, B., Henne, S., and Emmenegger, L.: Tracking isotopic signatures of CO_2 at the high altitude site Jungfraujoch with laser spectroscopy: Analytical improvements and representative results, Atmospheric Measurement Techniques, 6, 1659–1671, https://doi.org/10.5194/amt-6-1659-2013, 2013.

Tuzson, B., Mohn, J., Zeeman, M. J., Werner, R. A., Eugster, W., Zahniser, M. S., Nelson, D. D., McManus, J. B., and Emmenegger, L.: High precision and continuous field measurements of δ^{13}C and δ^{18}O in carbon dioxide with a cryogen-free QCLAS, Applied Physics B: Lasers and Optics, 92, 451–458, https://doi.org/10.1007/s00340-008-3085-4, 2008.

Tuzson, B., Henne, S., Brunner, D., Steinbacher, M., Mohn, J., Buchmann, B., and Emmenegger, L.: Continuous isotopic composition measurements of tropospheric CO_2 at Jungfraujoch (3580 m a.s.l.), Switzerland: Real-time observation of regional pollution events, Atmospheric Chemistry and Physics, 11, 1685–1696, https://doi.org/10.5194/acp-11-1685-2011, 2011.

Tuzson, B., Graf, M., Ravelid, J., Scheidegger, P., Kupferschmid, A., Looser, H., Morales, R. P., and Emmenegger, L.: A compact QCL spectrometer for mobile, high-precision methane sensing aboard drones, Atmospheric Measurement Techniques Discussions, 2020, 1–16, https://doi.org/10.5194/amt-2020-102, https://www.atmos-meas-tech-discuss.net/amt-2020-102/, 2020.

UNFCCC: Kyoto Protocol to the United Nations Framework Convention on Climate Change, http://unfccc.int/resource/docs/convkp/kpeng.pdf, 1998.

UNFCCC: Paris Agreement, https://unfccc.int/files/essential_background/convention/application/pdf/english_paris_agreement.pdf, 2015.

https://doi.org/10.5194/amt-2020-279
Preprint. Discussion started: 14 August 2020

Van Der Laan-Luijkx, I. T., Van Der Laan, S., Uglietti, C., Schibig, M. F., Neubert, R. E. M., Meijer, H. A. J., Brand, W. A., Jordan, A., Richter, J. M., Rothe, M., and Leuenberger, M. C.: Atmospheric CO_2, $\delta(O_2/N_2)$ and $\delta^{13}CO_2$ measurements at Jungfraujoch, Switzerland: Results from a flask sampling intercomparison program, Atmospheric Measurement Techniques, 6, 1805–1815, https://doi.org/10.5194/amt-6-1805-2013, 2013.

Wendeberg, M., Richter, J. M., Rothe, M., and Brand, W. A.: Jena Reference Air Set (JRAS): a multi-point scale anchor for isotope measurements of CO_2 in air, Atmos. Meas. Tech., 6, 817–822, https://doi.org/10.5194/amt-6-817-2013, 2013.

Werle, P.: Accuracy and precision of laser spectrometers for trace gas sensing in the presence of optical fringes and atmospheric turbulence, Applied Physics B: Lasers and Optics, 102, 313–329, https://doi.org/10.1007/s00340-010-4165-9, 2011.